

Article

Wavelength Conversion Process of Intra-Pulse Stimulated Raman Scattering in Near-Zero Negative Dispersion Range

Bowen Chen ^{1,2}, Silun Du ^{1,2}, Deqi Li ^{1,2}, Baoqun Li ^{1,2}, Sunde Wang ^{1,2} and Tianshu Wang ^{1,2,*}

¹ Chongqing Research Institute, Changchun University of Science and Technology, Chongqing 401135, China; 2020200057@mails.cust.edu.cn (B.C.); silundu@mails.cust.edu.cn (S.D.); lidq@mails.cust.edu.cn (D.L.); libaoqun@mails.cust.edu.cn (B.L.); wangsd@mails.cust.edu.cn (S.W.)

² National and Local Joint Engineering Research Center of Space Optoelectronics Technology, Changchun University of Science and Technology, Changchun 130022, China

* Correspondence: wangts@cust.edu.cn

Abstract: In the near-zero negative dispersion region of highly nonlinear fiber, the process of wavelength conversion based on the mechanism of intra-pulse stimulated Raman scattering is sensitive to the parameters of pumping pulse and fiber length under the combined effects of nonlinearity and dispersion. Therefore, we experimentally demonstrate the process in detail by using conventional soliton pulses with three sets of pulse parameters and two highly nonlinear fiber lengths of 400 m and 500 m. The experimental results show that, under the combined action of dispersion and several types of nonlinear mechanisms, the wavelength conversion processes are apparently different when using pulses with different parameters to pump different lengths of highly nonlinear fibers. Specifically, the separation degree of the frequency-shifted pulse spectrum and pumping pulse spectrum, and the corresponding redshift rate and pump power consumption all show significantly different results. The experimental results can guide the selection of more suitable parameters for the pumping pulse and the length of highly nonlinear fiber to achieve a better effect of wavelength redshift or spectrum broadening for various practical applications.

Keywords: ultrashort mode-locked pulse; intra-pulse stimulated Raman scattering; highly nonlinear fiber; zero-negative dispersion region



Received: 29 November 2024

Revised: 18 January 2025

Accepted: 22 January 2025

Published: 23 January 2025

Citation: Chen, B.; Du, S.; Li, D.; Li, B.; Wang, S.; Wang, T. Wavelength Conversion Process of Intra-Pulse Stimulated Raman Scattering in Near-Zero Negative Dispersion Range. *Photonics* **2025**, *12*, 104. <https://doi.org/10.3390/photronics12020104>

Copyright: © 2025 by the authors. Licensee MDPI, Basel, Switzerland. This article is an open access article distributed under the terms and conditions of the Creative Commons Attribution (CC BY) license (<https://creativecommons.org/licenses/by/4.0/>).

1. Introduction

In 1986, F. M. Mitschke and L. F. Mollenauer discovered the phenomenon of soliton self-frequency shift (SSFS) [1]; soon afterward, Gordon interpreted it as an effect caused by intra-pulse stimulated Raman scattering (ISRS) [2]. The frequency shift range of SSFS is proportional to the transmission distance and fourth power of the reciprocal of the temporal width of the pulse [2]. Therefore, pumping pulses with temporal widths of picosecond or sub-picosecond are usually utilized to guarantee the wavelength shift range [3–10]. The fiber types commonly utilized include single-mode silica fiber [3,5,9], photonic crystal fiber (PCF), or a PCF with a large mode field area in the polarization control method [7,10], and mid-infrared fiber [4,6,8]. The span of the wavelength shift can range from 400 nm to 3.35 μm [4,5]. The effects of SSFS have been applied in various fields, including optical delay line [11], optical analog-to-digital conversion [12–14], fiber sensing [15,16], and optical coherence tomography [17].

For SSFS studies, usually, a pumping pulse with fixed parameters of pulse width and spectral width and a highly nonlinear fiber (HNLF) with a kilometer length and low negative dispersion coefficient are utilized to achieve a large Raman frequency shift [11–14].

However, first, long fibers will broaden the temporal width of the pumping pulse and frequency-shifted pulse under the effect of group velocity dispersion (GVD) [18], and inhibit the further frequency shift due to the inverse relationship between the Raman frequency shift, Raman gain, and pulse width [2,19]. Hence, it is reasonable to consider pumping the near-zero negative dispersion range of HNLF to decrease the temporal broadening rate of the pumping pulse and frequency-shifted pulse. Second, when utilizing a pumping pulse with a broader spectrum, the short-wavelength component of the pulse will provide more Raman gain to the long wavelength [1], which may be helpful to further increase the frequency shift range at the same input peak power and fiber length. Nevertheless, there are some potential problems that must be considered before making these attempts. First, spectrum-broadening more easily occurs at the near-zero dispersion position under the combined influences of nonlinear effects, such as four-wave mixing (FWM) and self-phase modulation (SPM) [20], which may decrease the separation degree and separation speed between the Raman frequency-shifted spectrum and pumping pulse spectrum. Second, the FWM and SPM processes also compete with the ISRS process for nonlinear gain, which can further suppress the process in which the pumping pulse provides Raman gain to longer wavelengths and the generation of a larger redshift wavelength becomes difficult. Therefore, the specific effect on the wavelength conversion process based on the ISRS mechanism is closely related to the pulse parameters and fiber length. And a detailed experimental observation is needed to explore these situations and provide a meaningful reference for different application scenarios requiring different wavelength conversion effects. As far as we know, there has been no such research.

In this paper, we utilized a conventional soliton pulse with three sets of pulse parameters of temporal and spectral widths to pump the HNLF in the near-zero negative dispersion region with two lengths of 400 m and 500 m. The temporal widths of the pumping pulse were set to 445 fs, 554 fs, and 318 fs, and the corresponding spectral widths were 8.56 nm, 9.82 nm, and 11.30 nm. When the peak power of the pumping pulse was set within 1.5 mW, the experimental results showed that, first, when the spectral width was set to 8.56 nm and 9.82 nm, the spectrum gradually exhibited a pronounced redshift wavelength from the pumping pulse wavelength with increasing peak power. Additionally, with a broader spectral width of 9.82 nm, even the temporal width of the pumping pulse was broader at 554 fs, and the range of wavelength redshift further expanded at a similar peak power and the same fiber length, accompanied by a faster rate of wavelength redshift and more pump power consumption. Moreover, with a longer HNLF of 500 m, the difference in the rate of wavelength redshift at these two spectral widths became more prominent. For the parameters, combinations of pumping pulses and HNLF lengths of 445 fs–8.56 nm–400 m, 554 fs–9.82 nm–400 m, 445 fs–8.56 nm–500 m, and 554 fs–9.82 nm–500 m, the corresponding rates of wavelength redshift were 3.16 nm/W, 4.16 nm/W, 3.83 nm/W, and 5.80 nm/W, respectively. The maximum redshift wavelength was achieved with the parameters of 554 fs–9.82 nm–500 m. Finally, when the spectral width of the pumping pulse was set to 11.30 nm with a shorter pulse width of 318 fs, the effect of ISRS was suppressed to a certain extent and the largest redshift wavelength also decreased for the two fiber lengths compared with the previous two sets of pulse parameters. In addition, the separation degree between the frequency-shifted spectrum and the pumping pulse spectrum decreased, and the top of the frequency-shifted spectrum gradually exhibited a flatter, broadening shape with increasing peak power. The results were caused by the nonlinear effects of FWM and enhanced SPM. For the application scenarios mentioned before, this experimental research can provide a meaningful reference for the reasonable selection of pulse parameters and length of HNLF to achieve a better effect of wavelength redshift or spectrum broadening based on the ISRS process.

2. Experimental Setup and Operating Principle

Figure 1 shows a schematic of the experimental setup. The pulse source was an er-doped mode-locked fiber laser based on the nonlinear multimode interference effect using a graded index multimode fiber (GIMF), as shown in Figure 1a. It can operate stably in the single-soliton pulse state. Figure 1b shows the experimental setup's optical link for observing the wavelength conversion process of intra-pulse stimulated Raman scattering. First, the soliton pulse was coupled into a chirped pulse amplification system (CPA) consisting of a section of dispersion compensation fiber (DCF), an erbium-doped fiber amplifier (EDFA), and a section of single-mode fiber (SMF) to obtain a pulse with relatively higher peak power and sub-picosecond temporal width. The length of the DCF and SMF in the CPA system were approximately 10 m and 50 m, respectively. The GVD of DCF and SMF at 1550 nm were approximately $180 \text{ ps}^2/\text{km}$ and $-22.94 \text{ ps}^2/\text{km}$, respectively. The EDFA was set to three different amplification powers to induce varying degrees of nonlinear spectral broadening during the amplification process for the soliton pulse. The function of the polarization-independent optical isolator (PI-ISO) is to prevent the reflected light from entering the EDFA, thereby avoiding any adverse impact on operational performance. Second, after outputting from the CPA system, a variable optical attenuator (VOA) was used to control the power of the soliton pulse entering the HNLF through the optical fiber coupler (OC). One percent power was utilized to monitor the power of the pulse entering the HNLF, and the ISRS processes in the HNLF with two lengths of 400 m and 500 m were observed. Because the core of HNLF is smaller than SMF, there is a certain mode field mismatch loss when the two kinds of fiber are fused. Therefore, the insertion loss of the HNLF with two lengths was tested under the condition with almost the same welding operation, which were both about 2.70 dB. The GVD of the HNLF was approximately $0 \text{ ps}^2/\text{km}$ at 1550 nm, and the nonlinear coefficient was approximately $10 \text{ W}^{-1}/\text{km}$. Finally, the experimental results of wavelength conversion processes based on the ISRS process were observed by an optical spectrum analyzer (OSA, YOKOGAWA AQ6375).

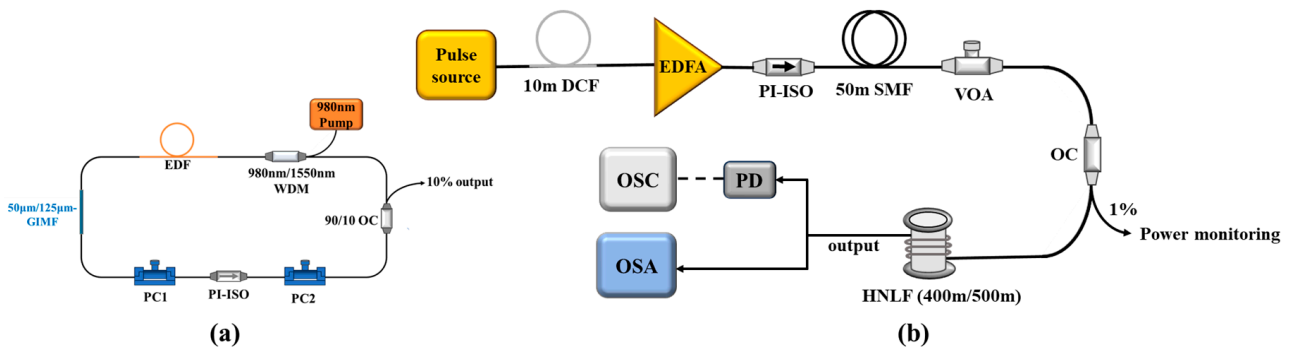


Figure 1. (a) Structure diagram of the pulse source. (b) Optical experiment link for the wavelength conversion process of intra-pulse stimulated Raman scattering.

3. Results and Analysis

3.1. Preparation of Pumping Pulses with Different Parameters

Figure 2 shows graphs of the conventional soliton pulse source generated by the mode-locked structure as shown in Figure 1a. Figure 2a exhibits the spectrum with the typical characteristics of a conventional soliton pulse, which displays nearly symmetrical sidebands for the central wavelength near 1562.0 nm. These sidebands are called Kelly sidebands and are caused by resonant enhancement between the dispersive wave (DW) and soliton pulse [21]. Figure 2b shows a pulse train in the time domain span of 800 ns, where the spacing between each pulse is approximately 41.86 ns, corresponding to a fundamental repetition frequency of approximately 23.890 MHz, which is basically consistent

with the radio frequency spectrum, as shown in Figure 2c, and the signal-to-noise of the fundamental radio frequency is 56.25 dB. The inset shows the radio frequency spectrum with uniform frequency spacing measured in a frequency span of 500 MHz. The SNR and the inset indicated that the mode-locked fiber laser could operate stably. In order to obtain soliton pulses with three different spectral widths and the corresponding temporal widths, the EDFA was set to three different amplifying powers to induce different degrees of nonlinear spectral broadening during the amplification process for the soliton pulse. As shown in Figure 3a, the three different spectral widths were adjusted to 8.56 nm, 9.82 nm, and 11.30 nm, respectively, and the pumping pulse had approximately the same central wavelength at 1562.0 nm. Before amplification, the spectral intensity of the Kelly sideband was suppressed by finely setting the angle of the PCs and the length of the graded-index multimode fiber in the fiber resonator in order to keep the sidelobe suppression ratio between the central wavelength and the Kelly sideband above 8 dB for each amplified spectrum. Thus, the amplified soliton pulses can achieve the favorable effect of temporal compression. For the amplified soliton pulses with three spectral widths, 50 m SMF was used for compression, as shown in Figure 1b. The measured pulse widths were 445 fs, 554 fs, and 318 fs, respectively, as shown in Figure 3b, according to the autocorrelator test and hyperbolic secant fitting. According to the time–bandwidth product (TBP) theory, in general, $\tau_p \Delta\nu > \kappa$, where τ_p is the pulse half-height full width in the time domain and $\Delta\nu$ is the half-height full width of the optical frequency obtained by Fourier transformation of τ_p . Because the time domain distribution of the conventional soliton pulse is hyperbolic secant, $\kappa = 0.315$, the Fourier transformation limited pulse durations corresponding to the three different spectral widths of 8.56 nm, 9.80 nm, and 11.30 nm were calculated to be about 299 fs, 261 fs, and 227 fs, respectively, indicating that the compressed pump pulses still retain large residual chirp, it is especially true for pump pulses with a spectral width of 9.80 nm. This is because, in order to obtain different pump pulse parameters to study the ISRS process, its compression effect is artificially reduced by adjusting the state of the 50 m SMF. Next, they were utilized to stimulate the wavelength conversion processes based on intra-pulse stimulated Raman scattering in the near-zero negative dispersion region of HNLFs with two lengths of 400 m and 500 m. The dispersion coefficient of HNLF at 1562 nm was approximately $-0.364 \text{ ps}^2/\text{km}$.

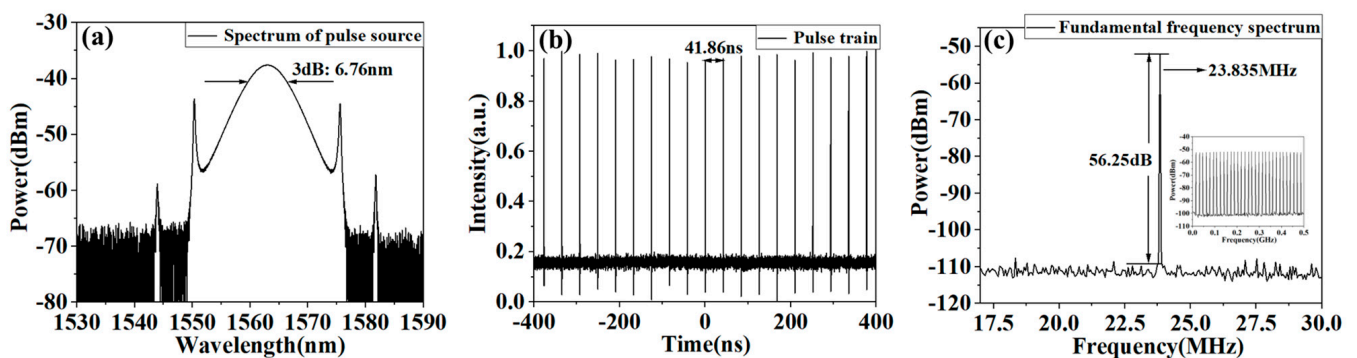


Figure 2. Data graphs of conventional soliton pulse source. (a) Spectrum of pulse source. (b) Pulse train in the time domain. (c) Radio frequency spectrum of pulse source.

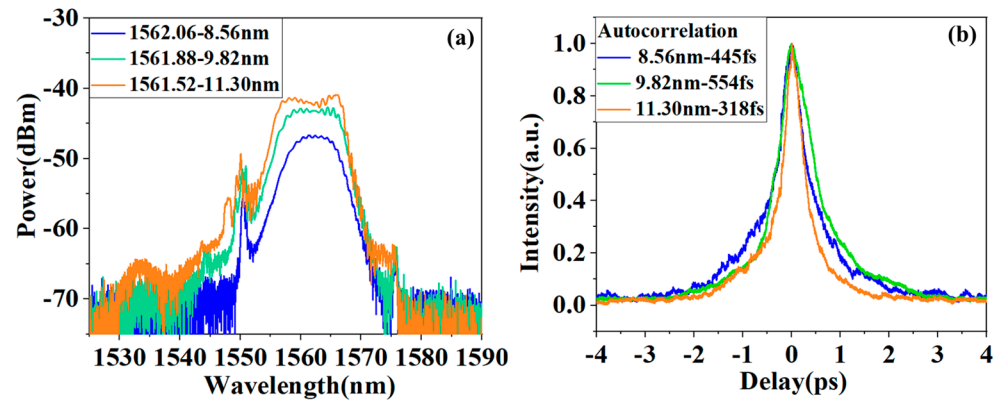


Figure 3. (a) Soliton pulses with different spectral widths after amplification. (b) Corresponding pulse widths after compression.

3.2. Wavelength Conversion Processes in Highly Nonlinear Fiber with the Two Lengths of 400 m and 500 m Pumped by a Soliton Pulse with 8.56 nm Spectral Width and 445 fs Temporal Width

First, the wavelength conversion processes based on the ISRS effect in HNLFs with two lengths of 400 m and 500 m were observed using a soliton pulse with a spectral width of 8.56 nm and pulse width of 445 fs. Figure 4a shows the results for the 400 m HNLF. As the input peak power of the pumping pulse increased gradually, a progressively pronounced wavelength redshift emerged on the longer wavelength side to the amplified pumping pulse wavelength which was observed after EDFA and was as shown as the red solid line, which was attributed to the ISRS effect. When the peak power increased to 15.44 W considering the estimated splicing loss of 2.50 dB, a separation wavelength position at 1579.8 nm appeared between the extended frequency-shifted spectrum and the pumping pulse spectrum. For the application fields, such as optical analog-to-digital conversion [12–14] and optical fiber sensing [15,16], the spectral components used were precisely such extended frequency-shifted spectrum. The extension of the wavelength redshift exhibited a progressive increase with the increasing input peak power due to the relationship between the Raman frequency shift and the peak power of the pumping pulse that was expressed as $\Delta\omega = -8T_R\gamma P_0 / (15T_0^2)$ [15], where T_R is a constant independent of the wavelength and originates in the Raman-delayed response, γ is the nonlinear coefficient of the fiber, and P_0 and T_0 are the peak power and temporal width of the pumping pulse, respectively. The maximum frequency-shifted wavelength was 1643.3 nm when the peak power was 30.78 W. In addition, the spectral width of the pumping pulse gradually widened, and a multi-peak structure appeared in the pumping pulse spectrum and the frequency-shifted spectrum. This should be due to the self-phase modulation (SPM) process of the pumping pulse and frequency-shifted pulse, and the generation of the multi-peak structure was due to the constructive interference and destructive interference between different spectral components [22]. When the fiber length was 500 m, the process of spectral redshift was generally similar to that of 400 m, as shown in Figure 4b. The differences were that, on the one hand, the wavelength separation position between the frequency-shifted spectrum and the pump spectrum slightly decreased to 1577.1 nm at the lower peak power of 9.57 W. On the other, the maximum frequency-shifted wavelength increased to 1666.9 nm when the peak power was 30.84 W. The reason for the reduction in the wavelength separation position was likely the longer fiber length providing larger Raman gain for the redshift wavelength and causing the frequency-shifted spectrum to build up more quickly, according to the exponential relationship between the intensity of the frequency-shifted spectrum and the fiber length, which was expressed as $\exp(gL)$ [23], where g is the Raman gain coefficient and L is the fiber length. As for the increase in the maximum frequency-shifted wavelength, it was due to the dependent relationship of the Raman frequency shift on the

transmission distance that was expressed as $\Delta\omega = 8T_R|\beta_2|z/(15T_0^4)$ [15], where β_2 is the second-order group velocity dispersion coefficient of the transmission fiber and z stands for the transmission distance.

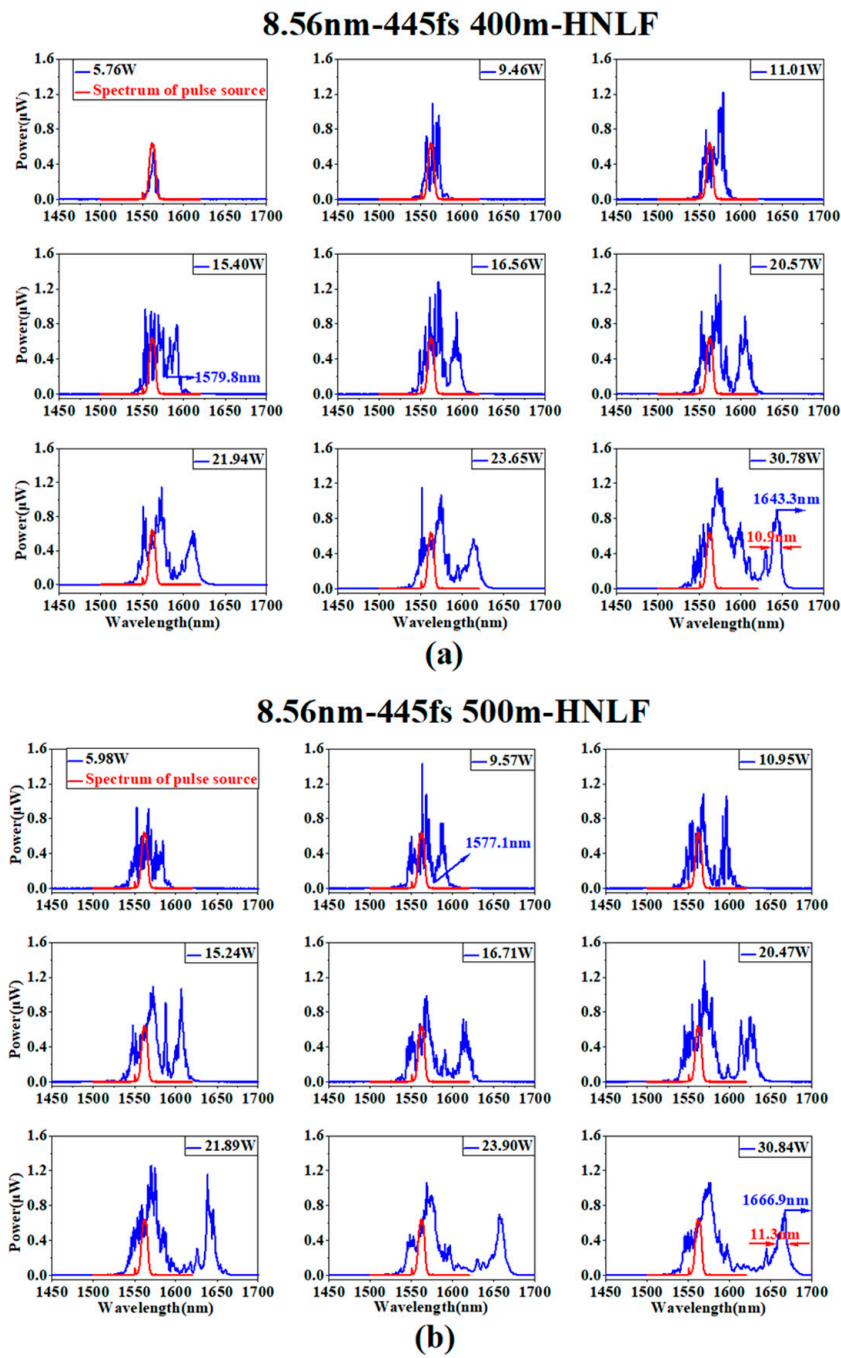


Figure 4. Wavelength conversion processes of intra-pulse stimulated Raman scattering in highly nonlinear fiber with two lengths of (a) 400 m and (b) 500 m pumped by a soliton pulse with a spectral width of 8.56 nm and pulse width of 445 fs.

3.3. Wavelength Conversion Processes in Highly Nonlinear Fiber with the Two Lengths of 400 m and 500 m Pumped by a Soliton Pulse with 9.82 nm Spectral Width and 554 fs Temporal Width

Next, a soliton pulse with a spectral width of 9.82 nm and pulse width of 554 fs was utilized as the pumping pulse, and the results of wavelength conversion processes are as shown in Figure 5. For the fiber length of 400 m, it can be seen from Figure 5a that, when the peak power increased from 12.27 W to 25.99 W, two robust spectral components

nearly appeared symmetrically on the two sides of the pumping pulse spectrum. The right spectral components were 1588.2 nm, 1589.3 nm, 1589.9 nm, and 1588.5 nm, respectively. It likely originated from the degenerate FWM process of the pumping pulse [22], where the pumping light with an optical frequency of w_1 produced two symmetrical side bands with optical frequencies of w_3 and w_4 . Assuming that $w_3 < w_4$, the frequency shift is expressed as $\Omega_s = w_1 - w_3 = w_4 - w_1$, where the higher frequency w_4 is called the anti-stokes band and the lower frequency w_3 is called the stokes band, corresponding to the right spectral components. The generation of the FWM process requires that the pumping light approximately meets a phase-matching condition that is $\kappa = \Delta k_M + \Delta k_W + \Delta k_{NL} \approx 0$, where Δk_M , Δk_W , and Δk_{NL} are the contributions to the phase mismatch corresponding to material dispersion, waveguide dispersion, and the nonlinear effect, respectively. Because HNLF is a type of single-mode fiber, the contribution of waveguide dispersion Δk_W can be ignored. In the near-zero negative dispersion range, the contribution of material dispersion Δk_M is a small negative value related to the stokes optical frequency. Meanwhile, for the nonlinear contribution $\Delta k_{NL} = 2\gamma P_0$, it is a positive value. It can be seen that the stokes wavelength position changes little with the increase in pumping powers. It should be noted that the spectral intensity of the pumping pulse changed little under the influence of soliton self-frequency shift. For quartz fiber, the gain of FWM was greater than the Raman scattering [23]. Therefore, the FWM process occurred first and inhibited the formation of a Raman frequency-shifted spectrum at lower peak powers, leading to slower separation between the extended frequency-shifted spectrum and pumping pulse spectrum, and the separation wavelength increased to 1595.9 nm compared with that, as Figure 4 shows. When the peak power increased to 45.97 W, the maximum frequency-shifted wavelength was 1742.0 nm. It is worth noting that the spectral component with a wavelength of 1619.8 nm should be the secondary Raman frequency-shifted spectrum excited by the fundamental soliton pulse generated from the splitting of the higher-order soliton formed by the pumping pulse with larger peak power in HNLF [24]. For the fiber length of 500 m, it can be seen from Figure 5b that the stokes wavelength produced by the FWM process nearly did not appear in the peak power range, similar to that shown in Figure 5a. This is because the change in core diameter made it difficult to maintain phase matching in the longer fiber length. It helped to separate the Raman frequency-shifted spectrum from the pumping pulse spectrum more quickly, and the wavelength separation position decreased to 1576.2 nm when the peak power was 11.99 W. The maximum frequency-shifted wavelength increased to 1775.0 nm at a peak power of 45.84 W due to the dependent relationship of the Raman frequency shift on the transmission distance, as mentioned above. In addition, compared with those at peak powers of 30.78 W and 30.84 W, as shown in Figure 4, the redshift wavelengths increased by 5.9 nm and 5.3 nm at the lower peak powers of 25.29 W and 25.11 W, respectively. The 3 dB bandwidths of the frequency-shifted spectrum were wider than that, as shown in Figure 4. This indicates that the frequency-shifted pulse obtained wider spectral gain, and the wider frequency-shifted spectrum corresponded to a narrower pulse width. Therefore, the redshift wavelengths increased a little according to the relationship of the Raman frequency shift with the pulse width. This is likely due to the short wavelength within the pumping pulse spectrum providing greater Raman gain for the redshift wavelength for the pumping pulse with a wider spectral width, as mentioned above.

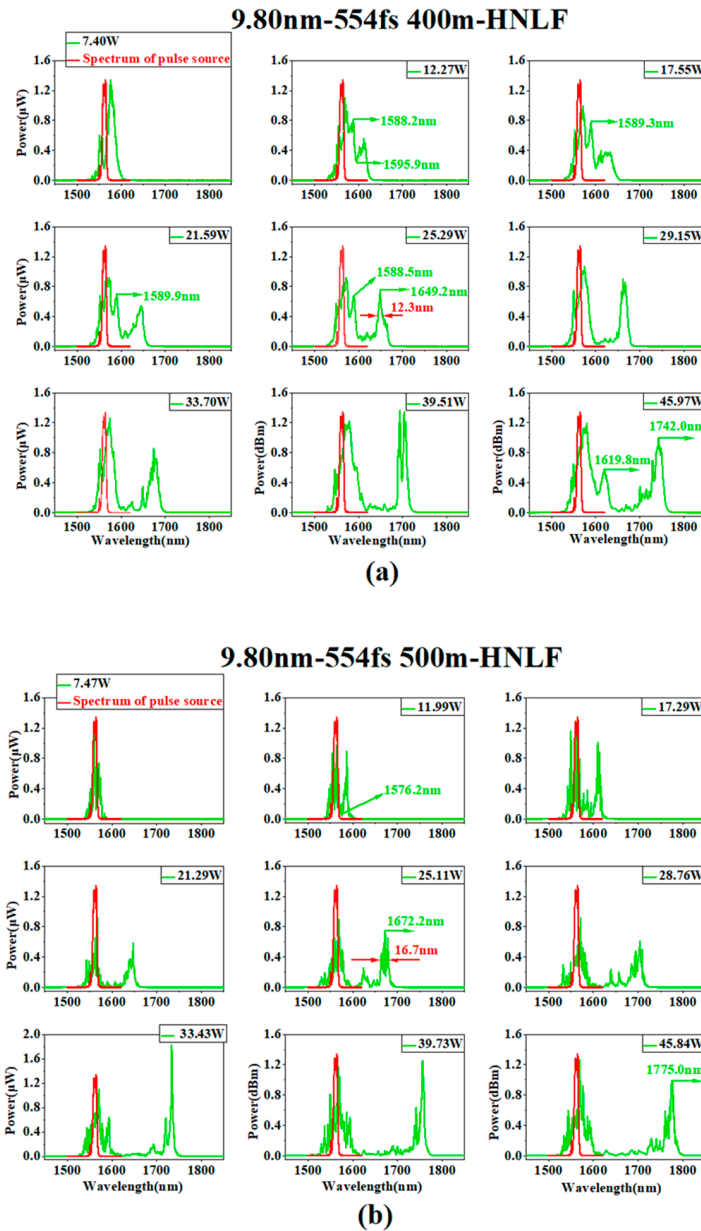


Figure 5. Wavelength conversion processes of intra-pulse stimulated Raman scattering in highly nonlinear fiber with two lengths of (a) 400 m and (b) 500 m pumped by the soliton pulse with a spectral width of 9.82 nm and pulse width of 554 fs.

3.4. Results of Raman Soliton Wavelength Redshift for the Pumping Pulse with the Two Sets of Parameters

As the input peak power of the pumping pulse with the two sets of parameters increased, the results of the wavelength redshift of the Raman soliton pulse for the two fiber lengths are as shown in Figure 6a. At the maximum input peak powers of 30.78 W, 45.97 W, 30.84 W, and 45.84 W, the corresponding largest redshift wavelengths were 1643.3 nm, 1742.0 nm, 1666.9 nm, and 1775.0 nm, respectively. They corresponded to pumping pulse and fiber lengths of 8.56 nm–400 m, 9.82 nm–400 m, 8.56 nm–500 m, and 9.82 nm–500 m, respectively. The corresponding wavelength redshift rates calculated by linear fitting were 3.16 nm/W, 4.16 nm/W, 3.83 nm/W, and 5.80 nm/W, respectively. It can be seen that, at the same fiber length, the wavelength redshift achieved a greater range at a similar peak power range and a faster rate utilizing the soliton pulse with a wider spectral width, indicating that it had higher pumping efficiency. Additionally, at the longer fiber length,

the differences in the range and the rate of the wavelength redshift became more evident with the two different spectral widths. These results can be attributed to the dependence of Raman gain on the spectral width of the pumping pulse and the exponential relationship between the Raman gain and fiber length. Figure 6b shows the power consumption results with the increasing peak power of the pumping pulse. The ratio between the pumping pulse's output power and input peak power represents an accelerated decrease with the increasing peak power, indicating that the power consumption of the pumping pulse increased with increasing peak power. Additionally, more power consumption originated from the pumping pulse with a wider spectral width and a longer fiber length. These results correspond well with that of the wavelength redshift.

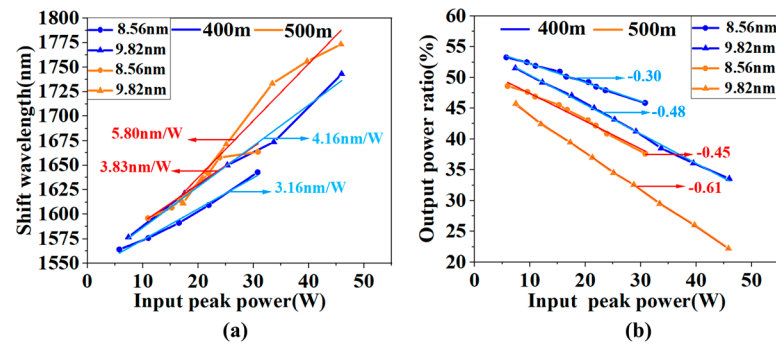


Figure 6. (a) Results of Raman soliton wavelength redshift for the pumping pulse with two sets of parameters. (b) Power consumption of pumping pulse for the two fiber lengths of 400 m and 500 m pumped by the pumping pulses with two parameters of 8.56 nm–445 fs and 9.82 nm–554 fs.

3.5. SSFS Processes in Highly Nonlinear Fiber with Two Lengths of 400 m and 500 m Pumped by the Soliton Pulse with 11.30 nm Spectral Width and 318 fs Temporal Width

Finally, the spectral and temporal width of the pumping pulse were set to 11.30 nm and 318 fs. As Figure 7 shows, on the whole, the redshift spectrum appeared at the higher peak power. The differences were that the largest redshift wavelengths were smaller than those in Figure 5, in which they were 1742.0 nm and 1775.0 nm, though with a shorter pulse width. The largest redshift wavelength with a fiber length of 400 m was 1734.2 nm larger than 1689.0 nm with a length of 500 m. Moreover, the pumping and frequency-shifted spectrums were wider than those shown in Figures 4 and 5 and evolved gradually to a flatter top with increasing peak power, especially for those as shown in Figure 7b, such spectral morphology is required for optical coherence tomography application [17]. The overall frequency-shifted spectrum separation degree diminished compared with the results as shown in Figures 4 and 5 by using the previous two sets of pulse parameters. The reason for the above results was likely due to a more complex process involving many physical mechanisms, such as the spectral broadening induced by SPM and FWM, and the enhanced temporal broadening of the wider pulse spectrum under the influence of dispersion. As for the SPM process, it could produce a phase shift related to the time distribution of the pulse intensity that was expressed as $\phi_{NL}(L, T) = |U(0, T)|^2 (L_{eff} / L_{NL})$ [22], where $U(0, T)$ is the light field amplitude of pumping pulse before entering into the fiber, $L_{eff} = (1/\alpha) [1 - e^{-\alpha L}]$ is the fiber effective length, α is the absorption coefficient, L is the actual length, $L_{NL} = 1/(\gamma P_0)$ is the nonlinear length, and P_0 is the peak power of the pumping pulse. In general, the maximum intensity of the pulse was located near the center of the time domain, and the corresponding maximum phase shift was $\phi_{max} = \gamma P_0 L_{eff}$. Therefore, the pumping pulse with the shorter width had higher peak power at a certain range of input power and experienced a larger phase shift in HNLF. This time-dependent phase shift process could create new frequency components that widened the spectrum of

the pumping pulse and frequency-shifted pulse. In addition, higher peak power may make the pulse closer to the phase-matching condition for the FWM process as mentioned above, which can also widen the spectrum. For the longer fiber length, the spectral broadening was more pronounced, which should be due to the stronger nonlinear processes; therefore, the spectral separation degree between the frequency-shifted spectrum and pumping pulse spectrum with 500 m HNLf was further diminished compared with that with 400 m HNLf. In addition, the oscillating structure in the spectrum of the pumping pulse and frequency-shifted pulse became less evident compared with that as shown in Figures 4 and 5, because the pumping pulse and frequency-shifted pulse carried a larger positive chirp in the time domain through the stronger SPM processes [22]. As for the reduced redshift wavelength, first, a wider spectrum can make the temporal width of frequency-shifted pulse widen faster under the influence of dispersion. Moreover, there was a nonlinear gain competition between the FWM process and ISRS process, which could inhibit the conversion between the pumping pulse spectrum and frequency-shifted pulse spectrum toward a longer redshift spectrum. Finally, the effect of self-steepening needs to be taken into account when the pulse with the narrower temporal width was used, which could also suppress the ISRS process [25].

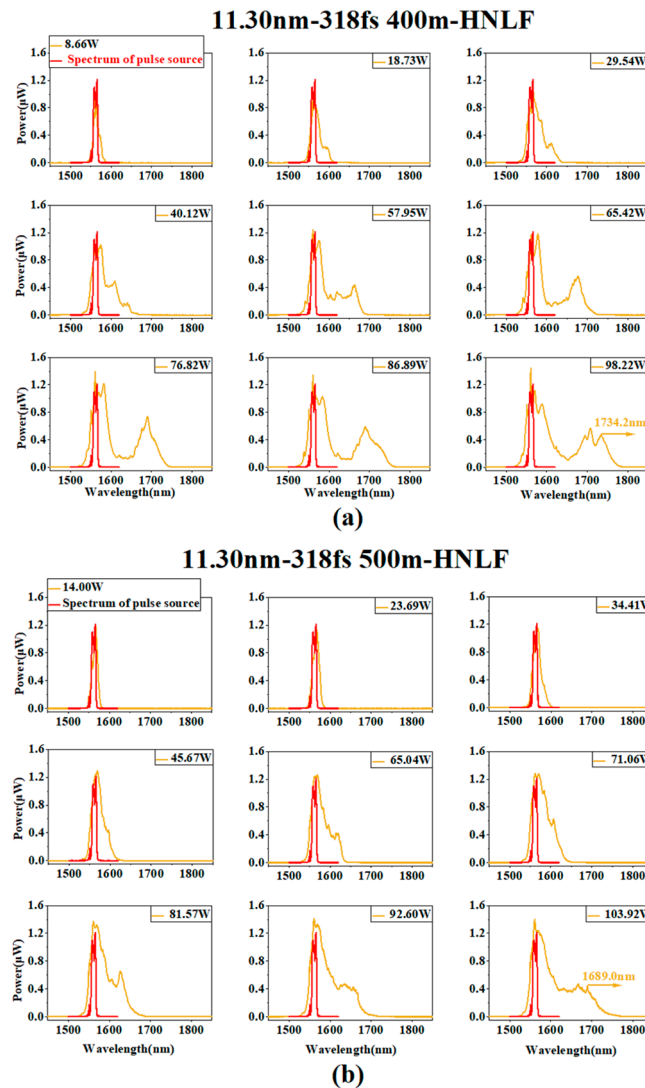


Figure 7. Wavelength conversion processes of intra-pulse stimulated Raman scattering in highly nonlinear fiber with two lengths of (a) 400 m and (b) 500 m pumped by the soliton pulse with a spectral width of 11.30 nm and pulse width of 318 fs.

3.6. Discussion

Table 1 shows the results of the wavelength redshift process based on the ISRS mechanism of two lengths of 400 m and 500 m HNLF pumped by the soliton pulse with three parameters. It can be seen that the wavelength redshift process is very sensitive to pumping pulse parameters and fiber length. The experimental results of the spectral separation speed and effect between the Raman frequency-shifted spectrum and the pumping pulse spectrum exhibited a great difference as the input peak power increased. Compared with the spectral separation effects between the Raman frequency-shifted spectrum and pumping pulse spectrum with pumping pulse parameters of 445 fs–8.56 nm and 554 fs–9.82 nm, the spectral separation effect with pulse parameters of 318 fs–11.30 nm was the worst. This is because the spectral width of the pumping pulse and frequency-shifted pulse were widened by the enhanced SPM and FWM effects with a higher peak power of the shorter pulse width, especially for the frequency-shifted spectrum with 500 m HNLF. For the pumping pulse parameter of 554 fs–9.82 nm and the HNLF length of 500 m, the spectral separation speed and separation effect were both the best due to the relationship between the spectral width of the pumping pulse and the fiber length and Raman gain. It was also related to the inability to produce an efficient FWM process due to the phase perturbation with the longer fiber length. The largest redshift wavelength and wavelength redshift rate were also achieved by this set of parameters; they were 1775.0 nm and 5.80 nm/W, respectively. However, due to the enhanced SPM and FWM effects with the shorter pulse width of 318 fs, the wider spectral width could make the temporal width of the Raman frequency-shifted pulse widen faster under the influence of dispersion. In addition, there was nonlinear gain competition between ISRS and FWM effects. And self-steepening effects also needed to be taken into account at the shorter pulse width. Therefore, under the combined influence of these factors, although the width of the pump pulse was narrower, the wavelength redshift range decreased.

Table 1. Comparison of the effect of wavelength redshift process based on ISRS mechanism.

Pulse Parameter	HNLF Length	Rank of Frequency-Shifted Spectrum Separation Speed	Wavelength Redshift Efficiency	Largest Redshift Wavelength
445 fs–8.56 nm	400 m	2nd	3.16 nm/W	1643.3 nm (30.78 W)
445 fs–8.56 nm	500 m	3rd	3.83 nm/W	1666.9 nm (30.84 W)
554 fs–9.82 nm	400 m	4th	4.16 nm/W	1742.0 nm (45.97 W)
554 fs–9.82 nm	500 m	1st	5.80 nm/W	1775.0 nm (45.84 W)
318 fs–11.30 nm	400 m	5th	\	1734.2 nm (98.22 W)
318 fs–11.30 nm	500 m	6th	\	1689.0 nm (103.92 W)

4. Conclusions

In this paper, we used the pulse with three different parameters of temporal and spectral widths to pump the HNLF in the near-zero negative dispersion region with two lengths of 400 m and 500 m, which were 445 fs–8.56 nm, 554 fs–9.82 nm, and 318 fs–11.30 nm. The experimental results of the wavelength conversion processes of ISRS were observed and analyzed in detail. The wavelength redshift processes were very different under the

combined influences, including the relationship between the spectral width of the pumping pulse and the fiber length and Raman gain, the FWM process of the pumping pulse, and the enhanced FWM and SPM effects for the pumping pulse and frequency-shifted pulse. The best Raman frequency shift effect was achieved by using the soliton pulse parameters of 9.82 nm spectral width, 554 fs temporal width, and 500 m HNLF, the largest redshift wavelength was 1775.0 nm, and the pumping efficiency was also the highest, at 5.80 nm/W. For the pumping pulse with the 11.30 nm spectral width and 318 fs temporal width, the combined processes of ISRS and enhanced FWM and SPM caused the Raman frequency-shifted spectrum to be flatter. These experimental results can provide a meaningful reference for the selection of pulse source parameters and fiber length for different application scenarios requiring different Raman wavelength redshift effects.

Author Contributions: Conceptualization, B.C. and S.D.; methodology, B.C. and S.D.; validation, B.C. and B.L.; formal analysis, T.W. and S.D.; investigation, D.L. and B.L.; resources, T.W.; data curation, B.C. and B.L.; writing—original draft preparation, B.C.; writing—review and editing, T.W. and S.W.; visualization, D.L. and B.L.; supervision, T.W.; project administration, T.W.; funding acquisition, S.D. and B.L. All authors have read and agreed to the published version of the manuscript.

Funding: Natural Science Foundation of Chongqing City (CSTB2022NSCQ-MSX1342) and the Natural Science Foundation of Jilin Province (20220508134RC, 20240101353JC).

Institutional Review Board Statement: Not applicable.

Informed Consent Statement: Not applicable.

Data Availability Statement: The raw data supporting the conclusions of this article will be made available by the authors on request.

Conflicts of Interest: The authors declare that they have no known competing financial interests or personal relationships that could have appeared to influence the work reported in this paper.

References

1. Mitschke, F.M.; Mollenauer, L.F. Discovery of the soliton self-frequency shift. *Opt. Lett.* **1986**, *11*, 659–661. [[CrossRef](#)] [[PubMed](#)]
2. Gordon, J.P. Theory of the soliton self-frequency shift. *Opt. Lett.* **1986**, *11*, 662–664. [[CrossRef](#)] [[PubMed](#)]
3. Anashkina, E.A.; Andrianov, A.V.; Koptev, M.Y.; Mashinsky, V.M.; Muravyev, S.V.; Kim, A.V. Generating tunable optical pulses over the ultrabroad range of 1.6–2.5 μm in GeO_2 -doped silica fibers with an Er: Fiber laser source. *Opt. Express* **2012**, *20*, 27102–27107. [[CrossRef](#)] [[PubMed](#)]
4. Cheng, T.; Usaki, R.; Duan, Z.; Gao, W.; Deng, D.; Liao, M.; Kanou, Y.; Matsumoto, M.; Misumi, T.; Suzuki, T.; et al. Soliton self-frequency shift and third-harmonic generation in a four-hole As_2S_5 microstructured optical fiber. *Opt. Express* **2014**, *22*, 3740–3746. [[CrossRef](#)] [[PubMed](#)]
5. Salem, R.; Jiang, Z.; Liu, D.; Pafchek, R.; Gardner, D.; Foy, P.; Saad, M.; Jenkins, D.; Cable, A.; Fendel, P. Mid-infrared supercontinuum generation spanning 1.8 octaves using step-index indium fluoride fiber pumped by a femtosecond fiber laser near 2 μm . *Opt. Express* **2015**, *23*, 30592–30602. [[CrossRef](#)] [[PubMed](#)]
6. Koptev, M.Y.; Anashkina, E.A.; Andrianov, A.V.; Dorofeev, V.V.; Kosolapov, A.F.; Muravyev, S.V.; Kim, A.V. Widely tunable mid-infrared fiber laser source based on soliton self-frequency shift in microstructured tellurite fiber. *Opt. Lett.* **2015**, *40*, 4094–4097. [[CrossRef](#)]
7. Tang, Y.; Wright, L.G.; Charan, K.; Wang, T.; Xu, C.; Wise, F.W. Generation of intense 100 fs solitons tunable from 2 to 4.3 μm in fluoride fiber. *Optica* **2016**, *3*, 948–951. [[CrossRef](#)]
8. Duval, S.; Gauthier, J.C.; Robichaud, L.R.; Paradis, P.; Olivier, M.; Fortin, V.; Bernier, M.; Piché, M.; Vallée, R. Watt-level fiber-based femtosecond laser source tunable from 2.8 to 3.6 μm . *Opt. Lett.* **2016**, *41*, 5294–5297. [[CrossRef](#)] [[PubMed](#)]
9. Delahaye, H.; Granger, G.; Gomes, J.T.; Lavoute, L.; Gaponov, D.; Ducros, N.; Fevrier, S. Generation of 35 kW peak power 80 fs pulses at 2.9 μm from a fully fusion-spliced fiber laser. *Opt. Lett.* **2019**, *44*, 2318–2321. [[CrossRef](#)]
10. Stoliarov, D.; Koviarov, A.; Korobko, D.; Galiakhmetova, D.; Rafailov, E. Fibre laser system with wavelength tuning in extended telecom range. *Opt. Fiber Technol.* **2022**, *72*, 102994. [[CrossRef](#)]
11. Oda, S.; Maruta, A. All-optical tunable delay line based on soliton self-frequency shift and filtering broadened spectrum due to self-phase modulation. *Opt. Express* **2006**, *14*, 7895–7902. [[CrossRef](#)] [[PubMed](#)]

12. Takahashi, K.; Matsui, H.; Nagashima, T.; Konishi, T. Resolution upgrade toward 6-bit optical quantization using power-to-wavelength conversion for photonic analog-to-digital conversion. *Opt. Lett.* **2013**, *38*, 4864–4867. [[CrossRef](#)] [[PubMed](#)]
13. Zhang, X.; Zhang, Z.; Wang, S.; Liang, D.; Li, H.; Liu, Y. High-resolution quantization based on soliton self-frequency shift and spectral compression in a bi-directional comb-fiber architecture. *Opt. Commun.* **2018**, *410*, 571–576. [[CrossRef](#)]
14. Zhang, X.; Zhang, Z.; Wang, B.T. Optical quantization based on soliton self-frequency shift and a flexible spectrum compression scheme utilizing time-dependent filtering. *Opt. Express* **2019**, *27*, 21435–21447. [[CrossRef](#)] [[PubMed](#)]
15. Chen, X.; Sun, Y.; Gao, Y.; Yan, X.; Zhang, X.; Wang, F. Temperature sensing in a silica microstructured optical fiber based on soliton self-frequency shift. *IEEE Trans. Instrum. Meas.* **2021**, *70*, 9514409. [[CrossRef](#)]
16. Chen, X.; Yan, X.; Zhang, X.; Wang, F.; Suzuki, T.; Ohishi, Y.; Cheng, T. Highly sensitive nonlinear temperature sensor based on soliton self-frequency shift technique in a microstructured optical fiber. *Sens. Actuators A Phys.* **2022**, *334*, 113333. [[CrossRef](#)]
17. Sordillo, L.A.; Pu, Y.; Pratavieira, S.; Budansky, Y.; Alfano, R.R. Deep optical imaging of tissue using the second and third near-infrared spectral windows. *J. Biomed. Opt.* **2014**, *19*, 056004. [[CrossRef](#)] [[PubMed](#)]
18. Chestnut, D.A.; Taylor, J.R. Soliton self-frequency shift in highly nonlinear fiber with extension by external Raman pumping. *Opt. Lett.* **2003**, *28*, 2512–2514. [[CrossRef](#)]
19. Judge, A.C.; Bang, O.; Eggleton, B.J.; Kuhlmeier, B.T.; Mägi, E.C.; Pant, R.; de Sterke, C.M. Optimization of the soliton self-frequency shift in a tapered photonic crystal fiber. *J. Opt. Soc. Am. B-Opt. Phys.* **2009**, *26*, 2064–2071. [[CrossRef](#)]
20. Wadsworth, W.J.; Joly, N.; Knight, J.C.; Birks, T.A.; Biancalana, F.; Russell, P.S.J. Supercontinuum and four-wave mixing with Q-switched pulses in endlessly single-mode photonic crystal fibres. *Opt. Express* **2004**, *12*, 299–309. [[CrossRef](#)]
21. Kelly, S. Characteristic sideband instability of periodically amplified average soliton. *Electron. Lett.* **1992**, *28*, 806–808. [[CrossRef](#)]
22. Agrawal, G. *Nonlinear Fiber Optics*, 5th ed.; Academic Press: New York, NY, USA, 2013.
23. Stolen, R. Phase-matched-stimulated four-photon mixing in silica-fiber waveguides. *IEEE J. Quantum Electron.* **1975**, *11*, 100–103. [[CrossRef](#)]
24. Beaud, P.; Hodel, W.; Zysset, B.; Weber, H. Ultrashort pulse propagation, pulse breakup, and fundamental soliton formation in a single-mode optical fiber. *IEEE J. Quantum Electron.* **1987**, *23*, 1938–1946. [[CrossRef](#)]
25. Voronin, A.A.; Zheltikov, A.M. Soliton self-frequency shift decelerated by self-steepening. *Opt. Lett.* **2008**, *33*, 1723–1725. [[CrossRef](#)]

Disclaimer/Publisher’s Note: The statements, opinions and data contained in all publications are solely those of the individual author(s) and contributor(s) and not of MDPI and/or the editor(s). MDPI and/or the editor(s) disclaim responsibility for any injury to people or property resulting from any ideas, methods, instructions or products referred to in the content.